

# Non-linear metric perturbation enhancement of primordial gravitational waves

M. Bastero-Gil,<sup>1,2,\*</sup> J. Macias-Pérez,<sup>2,†</sup> and D. Santos<sup>2,‡</sup>

<sup>1</sup>*Departamento de Física Teórica y del Cosmos, Universidad de Granada, Granada-18071, Spain*

<sup>2</sup>*Laboratoire de Physique Subatomique et Cosmologie, Université Joseph Fourier Grenoble 1, CNRS/IN2P3, Institut Polytechnique de Grenoble, Grenoble-38026, France*

We present the evolution of the *full* set of Einstein equations during preheating after inflation. We study a generic supersymmetric model of hybrid inflation, integrating fields and metric fluctuations in a 3-dimensional lattice. We take initial conditions consistent with Einstein's constraint equations. The induced preheating of the metric fluctuations is not large enough to backreact onto the fields, but preheating of the scalar modes does affect the evolution of vector and tensor modes. In particular, they do enhance the induced stochastic background of gravitational waves during preheating, giving an energy density in general *an order of magnitude* larger than that obtained by evolving the tensors fluctuations in an homogeneous background metric. This enhancement can improve the expectations for detection by planned gravitational waves observatories.

keywords: cosmology, inflation, gravitational waves.

PACS numbers: 98.80.Cq, 04.25.D, 04.30.-w, 12.60.Jv

Cosmic microwave background (CMB) measurements [1], are consistent with an early period of inflation, which gives rise to the primordial curvature perturbation which seeds the large scale structure observed today. The observed power spectrum of temperature anisotropies is consistent with a Gaussian, adiabatic primordial spectrum, and present data sets at most an upper limit on the level of the primordial tensor contribution predicted by inflation. This contribution could be observed through B-mode polarization by the European Space Agency's Planck mission [2] and future CMB polarization experiments. Inflation should be followed by a reheating period, during which the inflationary vacuum energy is converted into radiation. During the first stages of reheating, the evolution of the system may be dominated by nonperturbative effects such as those of preheating, i.e., parametric amplification of quantum field fluctuations in a background of oscillating fields [3]. Through parametric resonance, field mode amplitudes grow exponentially within certain resonance bands in  $k$  space, this being an efficient way of transferring vacuum energy into radiation [3]. It does also enhance the tensor perturbations, sourced by the field anisotropic stress-energy tensor, giving rise to a stochastic background of gravitational waves (GWs) [4–6].

In most of the studies of preheating of GW, fields and tensor fluctuations are evolved in a background Friedmann-Robertson-Walker (FRW) metric. However, beyond linear perturbation, tensors are seeded by the other components of the metric, scalar and vectors [7]. Given that the metric and fields are nonlinearly coupled through the Einstein equations, the parametric amplification of field fluctuations will be rapidly transferred

to all metric perturbations. In a previous paper [8] we showed that this is indeed the case for the scalar metric perturbations. We showed that during the resonance the scalar metric source term for the tensors could be comparable to the anisotropic field stress tensor, arguing that they could affect the amplification of tensors. The purpose of this Letter is to show that this is indeed the case for hybrid models independently of model parameters. For that aim we have integrated the full set of Einstein equations, with the stress-energy tensor provided by the fields in hybrid inflation.

Einstein equations are written in the so-called Baumgarte-Shapiro-Shibata-Nakamura formalism [9], widely used because it provides a stable numerical evolution. One starts with the Arnowitt-Deser-Misner metric, given in terms of the lapse  $N$  and shift vector  $N^i$  functions, and the spatial metric  $\gamma_{ij}$ :

$$ds^2 = N^2 dt^2 - \gamma_{ij}(dx^i + N^i dt)(dx^j + N^j dt), \quad (1)$$

and performs a conformal transformation of the spatial metric,  $\tilde{\gamma}_{ij} = \exp(-4\beta)\gamma_{ij}$ , with  $\det\tilde{\gamma}_{ij} = 1$ . The metric dynamical variables are then  $\beta$  and  $\tilde{\gamma}_{ij}$ , the trace of the extrinsic curvature  $K = \tilde{\gamma}^{ij}K_{ij}$ , and its traceless part  $\tilde{A}_{ij} = \exp(-4\beta)(K_{ij} - \gamma_{ij}K/3)$ . In addition, a connection variable  $\tilde{\Gamma}^i = \tilde{\Gamma}_{jk}^i \tilde{\gamma}^{jk} = -\partial_j \tilde{\gamma}^{ji}$  is introduced in order to compute the Ricci curvature more accurately. The lapse and shift vector are gauge functions, and we choose to work in the synchronous gauge and set  $N = 1$  and  $N^i = 0$ . In this gauge we have  $K = 6\dot{\beta}$ , with  $\langle K \rangle/3 = H(t)$  being the average expansion rate, and  $\langle e^{2\beta} \rangle = a(t)$  the average scale factor ( " $\langle \cdot \rangle$ " denotes spatial average.). The spatial metric  $\tilde{\gamma}_{ij}$  encodes the two transverse and traceless degrees of freedom of the gravity waves, plus one additional scalar mode and 2 vector degrees of freedom, with  $\tilde{\gamma}_{ij} = 2\tilde{A}_{ij}$ .

The matter source is given by the stress-energy tensor of the two scalar fields (which we take as real scalar fields) in supersymmetric hybrid inflation, with potential

\*Electronic address: mbg@ugr.es

†Electronic address: macias@lpsc.in2p3.fr

‡Electronic address: santos@lpsc.in2p3.fr

$V(\phi, \chi) = V_0 + g^2 \chi^4 / 4 + g^2 (\Phi^2 - \phi_c^2) \chi^2 + m_\phi^2 \Phi^2 / 2$ , where  $\Phi$  is the inflaton field and  $\chi$  the waterfall field which triggers the phase transition at the end of inflation once the inflaton goes below the critical value  $\phi_c$ . The vacuum energy  $V_0$  is adjusted such that the potential vanishes at the global minimum,  $V_0 = g^2 \phi_c^4$ , and the mass for the inflaton field is set by the choice of the slow-roll parameter  $\eta_\phi = m_P^2 m_\phi^2 / V_0$ , where  $m_P$  is the reduced Planck mass.

The set of equations of motion are then given by the Klein-Gordon equations for the fields in the curved space given by the metric (1), the equations of motion for the connection  $\tilde{\Gamma}^i$ , and those for the metric variables [9] given by

$$\ddot{\beta} + 2\dot{\beta}^2 = \frac{1}{6m_P^2}(V - 2T) - \frac{1}{24}\dot{\gamma}_{ij}\dot{\gamma}^{ij}, \quad (2)$$

$$\ddot{\gamma}_{ij} + K\dot{\gamma}_{ij} = 2e^{-4\beta}(M_{ij}^{TF} - R_{ij}^{TF}) + \dot{\gamma}_j^k \dot{\gamma}_{ki}, \quad (3)$$

where  $T = (\dot{\Phi}^2 + \dot{\chi}^2)/2$  is the kinetic energy of the fields; the field-dependent source is  $M_{ij} = m_P^{-2}(\partial_i \Phi \partial_j \Phi + \partial_i \chi \partial_j \chi)$ ,  $R_{ij}$  is the Ricci tensor of the metric  $\gamma_{ij}$ , and the superscript “ $TF$ ” denotes the trace-free part of the tensor.

The system is placed in a finite and discrete 3D comoving box of length  $L$  and  $N$  sites per spatial dimension. The procedure introduces a comoving ultraviolet cut-off in both space and momentum. Ideally, one would like to keep both of them large enough: A big comoving box, larger than the initial Hubble size  $L > H(0)^{-1}$ , ensures that the observable initial Universe is within the box; but a large enough number of points is also required to have all the relevant momentum modes up to  $O(N/L)$ . For the problem of preheating after inflation, one tries to optimize the choice of this ratio  $O(N/L)$  to have an ultraviolet comoving momentum cut-off still larger than the preheating cut-off by the end of the simulation. This means that already at the start of the simulation our comoving box is smaller than the observable Universe, but the relevant physical modes for preheating are all included.

For the fields we follow the standard procedure, with the quantum field theory being replaced by an equivalent classical field theory. The quantum origin of the fields remains in the stochastic nature of the initial conditions<sup>1</sup>. We start the simulations some fraction of e-fold  $\Delta N_e = 0.05$  after the end of inflation, with the background inflaton field still close to the critical point,  $\langle \Phi \rangle = \phi_c \exp(-\eta_\phi \Delta N_e)$ , and its background velocity given by the slow-roll conditions<sup>2</sup>. The background val-

<sup>1</sup> A description of how to follow the quantum-to-classical transition for the scalar fields, and how to fix the initial conditions for the modes in the classical regime can be found in [10]. Nevertheless, we have checked that for the particular problem at hand, a better determination of the initial conditions has little impact on the results.

<sup>2</sup> For the model parameters considered, the inflaton field reaches

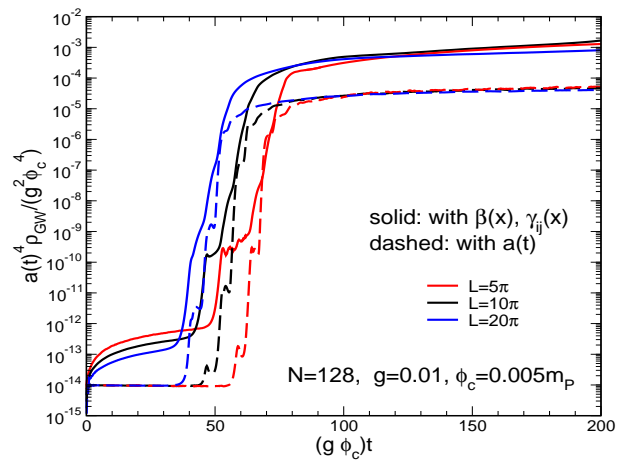


FIG. 1: Evolution of the energy density of GWs,  $\rho_{GW}$ , normalized by the initial vacuum energy  $\rho_i$ , for different values of the box size. Solid lines are the result of integrating the Einstein equations; dashed lines show the evolution of  $\rho_{GW}$  without including other metric fluctuations.

ues for the waterfall field are set to zero at this point. Classical inflaton field fluctuation in a spatial lattice with periodic boundary conditions are expanded as usual in Fourier modes  $\Phi_k$ , with an initial vacuum amplitude  $|\Phi_k(0)| \simeq 1/\sqrt{2\omega_k}$ , where  $\omega_k = \sqrt{k^2 + m_\phi^2}$ . The remaining variables must be chosen to satisfy the Einstein constraint equations, the momentum and the Hamiltonian constraint, at  $t = 0$ . This is the well known initial-value problem in general relativity [11]. We choose initially vanishing tensors and vectors, i.e.,  $\tilde{\gamma}_{ij}(0) = \delta_{ij}$ , such that the momentum constraint reduces to  $2\partial_i K = -(3/m_P^2)(\dot{\Phi}\partial_i\Phi + \dot{\chi}\partial_i\chi)$ . In order to fulfill this equation, we set the waterfall field as  $\chi(0) = \Phi(0) - \langle \Phi(0) \rangle$ , and<sup>3</sup>  $\dot{\chi}(0) = \langle \dot{\Phi}(0) \rangle - \dot{\Phi}(0)$ . This allows us to solve the momentum constraint for the initial value of the expansion rate fluctuations, and use the hamiltonian constraint to fix the fluctuations of the scale factor<sup>4</sup>.

Preheating in hybrid inflation models has been extensively studied in the literature [13]. The parametric amplification of the fluctuations takes place first through an

the critical point still in the slow-regime, and in the absence of any extra mechanism that could speed up the inflaton, slow-roll is a good approximation across the bifurcation point. For the dependency of the GW spectra on the initial velocity of the inflation field see [6].

<sup>3</sup> Given that once preheating starts the inflaton and waterfall fluctuations become comparable, results are independent of which field we set initially in the vacuum, and which is set by the constraint.

<sup>4</sup> Violations of the constraints are unavoidable during numerical integration, and their growth makes the system unstable. Numerically, we have checked that adding the covariant derivative of the momentum constraint in Eq. (2) renders the system more stable [12].

spinodal instability for the fields, during which the lower modes are quickly amplified. After a few oscillations, the amplitude of the fields has decayed enough to be out of the spinodal region, and tachyonic preheating ends. We just follow the evolution of the fields and metric variables up to the end of the resonance, before we lose the ultraviolet cut-off for the field modes. Metric variables will follow the same pattern of parametric amplification as the fields, with  $|\beta|^2 \sim m_P^{-2}|\Phi|^2$ . Keeping only the leading  $\beta$  terms in the Ricci tensor, we have:

$$R_{ij}^{TF} \simeq [-4\partial_i\beta\partial_j\beta + 2\partial_i\partial_j\beta]^{TF}, \quad (4)$$

and thus  $R_{ij}^{TF}$  becomes comparable to the field contribution  $M_{ij}^{TF}$  in Eq. (3).

The metric variable  $\tilde{A}_{ij}$  is traceless but nontransverse, i.e., it contains more degrees of freedom than those two corresponding to GWs. The traceless and transverse (TT) components are projected by using the operator [5]  $\Lambda_{ij,lm}(\hat{k}) = P_{il}(\hat{k})P_{jm}(\hat{k}) - P_{ij}(\hat{k})P_{lm}(\hat{k})/2$ , where  $P_{ij} = \delta_{ij} - \hat{k}_i\hat{k}_j$  and  $\hat{k}_i = k_i/k$ . The energy density of the GW is then  $\rho_{GW} = m_P^2 \langle \tilde{A}_{ij}^{TT}(t, x) \tilde{A}^{ij}(t, x) \rangle^{TT} = m_P^2 \int d^3k |\tilde{A}_{ij}^{TT}(t, k)|^2$  [4, 5]. In Fig. 1 we have plotted  $\rho_{GW}$ , normalized to the initial vacuum energy  $\rho_i = g^2\phi_c^4$ . We have taken as parameter models  $g = 0.01$ ,  $\phi_c = 0.005m_P$  and  $\eta_\phi = 0.05$ . The value of  $\rho_{GW}$  does not depend on the value of the coupling, which can be rescaled out from all the equations, but it does depend on the value of  $\phi_c$  [4–6], which sets the scale for the field source term<sup>5</sup> such that  $\rho_{GW}/\rho_i \propto \phi_c^2$ . We have included the results for different choices of the box size, to show that the final value of  $\rho_{GW}$  does not depend on the choice of  $L$  as far as we have all the relevant modes to start and end tachyonic preheating. With a larger comoving box we have more modes in the low momentum regime, and then tachyonic resonance starts slightly sooner, as can be seen in the plot.

We compare in Fig. 1 the results obtained when integrating the full Einstein equations (solid lines) with those obtained when integrating the tensor modes in a FRW background metric (dashed lines). The former are always roughly *an order of magnitude larger* due mainly to the contribution of the scalar modes of the metric fluctuations in Eq. (4). In Fig. 2, we show that both source terms,  $M_{ij}^{TF}$  and the leading term  $R_{ij}^{TF}$  in Eq. (4), are of the same order by the end of the resonance. Scalar metric fluctuations start growing immediately after inflation due to the increase in the kinetic energy of the field [see

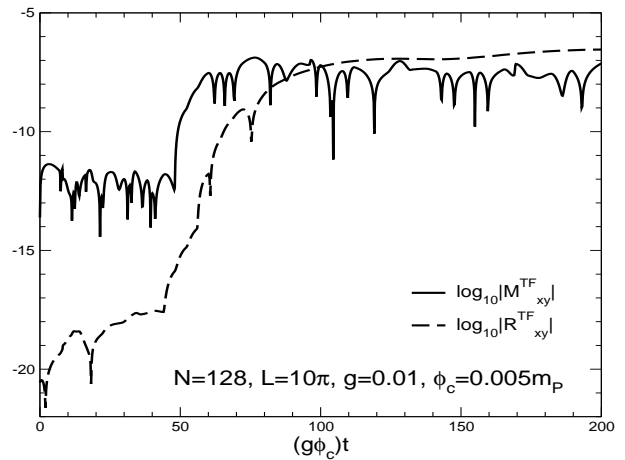


FIG. 2: Comparison of the evolution of the absolute values of the source terms  $M_{xy}^{TF}$  and  $R_{xy}^{TF}$  in Eq. (4), in logarithmic scale. The spikes in the plot are localized where the corresponding oscillating term vanishes.

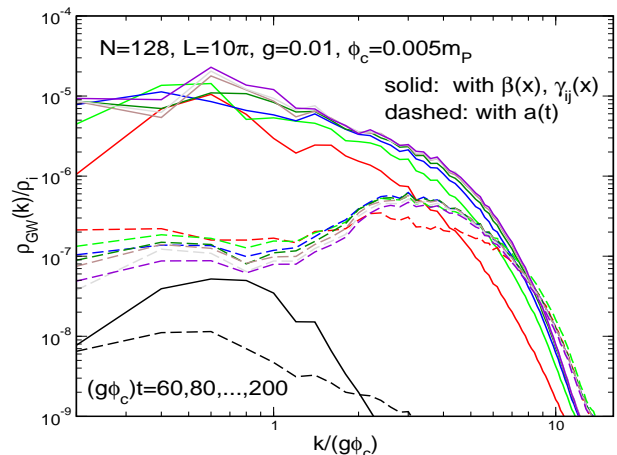


FIG. 3: Spectrum  $\rho_{GW}(k)/\rho_i$  per logarithmic  $k$  interval, for  $(g\phi_c)t = 60$  to 200 in intervals of 20 from bottom to top. Solid lines are the result of integrating the Einstein equations; dashed lines show the result of the integration in a FRW metric.

Eq. (2)], and this effect leads the initial growth of the tensor perturbations.

In Fig. 3, we show the spectrum of GW per logarithmic frequency interval,  $\rho_{GW}(k) = d\rho_{GW}/d\ln k$ , at different times until the end of the tachyonic resonance. Compared with the spectrum obtained without metric perturbations, the enhancement in the spectrum is localized at around the peak of the spectrum, shifted towards lower values at around  $k \simeq g\phi_c$ . This effect at low momenta is again due to the scalar metric perturbations, which spectrum peaks below  $g\phi_c$ . This can be seen in Fig. 4, where we compare the power spectra of the inflaton field fluctuations  $P_\phi = |\Phi(k)|^2$ , with those of the metric fluctuations  $\beta$  and  $A_{ij}^{TT}$ , at the end of the resonance. The field spectrum at  $t = 0$  is included as a

<sup>5</sup> The parameter  $\phi_c$  also sets the initial value of the expansion rate  $H_i/(g\phi_c) = \phi_c/(\sqrt{3}m_P)$ , and relatively large values of  $H_i$  have an impact on the evolution of the resonance, due to the fast redshifting of the field amplitudes. Tachyonic resonance ends once these amplitudes go below a certain value, and therefore the larger  $\phi_c$  and  $H_i$ , the shorter resonance time, and the smaller the amplification of the field fluctuations and, thus, of GWs.

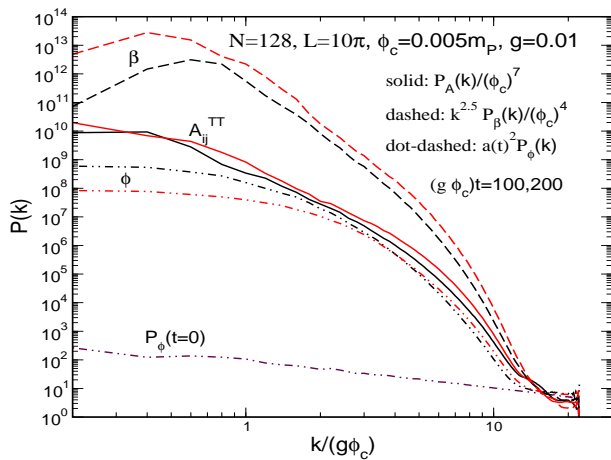


FIG. 4: Comparison of the power spectrum for the inflaton field  $P_\phi(k)$ , and metric perturbations  $P_\beta(k)$  and  $P_A$ , at  $(g\phi_c)t = 100$  (lower curves) and  $(g\phi_c)t = 200$  (upper curves). We have rescaled  $P_A$  by  $\phi_c^{-7}$  to have all the spectra in the same scale. For  $P_\beta$ , we have  $k^{2.5}P_\beta \simeq \phi_c^4 P_\phi$  from the momentum constraint at  $t = 0$  [8].

reference, to check that by the end of the simulation the highest momentum modes have not yet been amplified.

In summary, we have shown that nonlinear effects due to metric perturbations enhance the amplitude of the GW stochastic background by an order of magnitude with respect to the calculations in a FRW background metric. Taking into account that  $\rho_{GW}(k)$  is redshifted like radiation after the resonance, and assuming that entropy is conserved from reheating onwards, its maximum present-day value normalized by the critical density today is given by:

$$h^2 \Omega_{GW}^{peak} \simeq 5.5 \times 10^{-9} \left( \frac{\phi_c/m_P}{0.005} \right)^2 \left( \frac{T_{RH}^4}{\rho_i} \right)^{1/3}, \quad (5)$$

where  $T_{RH}$  is the reheating temperature at which the Universe becomes radiation-dominated. This amplitude is within the reach of the future GW observatory Advanced-LIGO for  $\phi_c \gtrsim 0.005m_P$ , or BBO for  $\phi_c \lesssim 0.005m_P$  [14]. However, today's values for the frequency are  $f = 6.4 \times 10^{10} \sqrt{g}[k/(g\phi_c)](T_{RH}/\rho_i^{1/4})^{1/3}$  Hz, while the operating frequency range for Advanced LIGO is  $1 - 10^3$  Hz, and BBO will operate in the range  $10^{-3} - 10^2$  Hz. Thus, to have the GW spectrum within the observable range, the coupling should be at most of the order of  $g \simeq 10^{-14}$ . The numerical simulations so far can resolve the spectrum for the typical frequency of the resonance,  $k \simeq g\phi_c$  and above, but not the infrared tail for subhorizon and superhorizon modes. The behavior of the GW spectrum in this infrared range and how they are affected by nonlinear metric effects is still an open question. A tail of subhorizon modes at the time of preheating rising slower than  $k^3$  could be detected by BBO, although  $f_{peak}$  were in the range of  $10^5$  Hz. Similarly, in models where the primordial curvature is enhanced during preheating [15], one could expect a similar effect for the tensor primordial spectrum, up to the level detectable in CMB polarization experiments.

We acknowledge for computing resources the IDRIS-CNRS (Babel) facility, and the cluster UGRGRID in Granada [16]. We have used the SUNDIALS package, “SUite of Nonlinear and Differential, ALgebraic equation Solver” [17] for the numerical integration.

- 
- [1] E. Komatsu et al., arXiv:1001.4538.  
[2] Planck: <http://www.rssd.esa.int/Planck>.  
[3] Y. Shtanov, J. Traschen and R. Brandenberger, Phys. Rev. **D 51** (1995) 5438; L. Kofman, A. Linde and A. A. Starobinsky, Phys. Rev. **D 56** (1997) 3258; D. I. Kaiser, Phys. Rev. **D 56** (1997) 706.  
[4] R. Easther, J. T. Giblin and E. A. Lim, Phys. Rev. Lett. **99** (2007) 221301; Phys. Rev. D **77** (2008) 103519.  
[5] J. García-Bellido and D. G. Figueroa, Phys. Rev. Lett. **98** (2007) 061302; J. Garcia-Bellido, D. G. Figueroa and A. Sastre, Phys. Rev. D **77** (2008) 043517.  
[6] J. F. Dufaux, A. Bergman, G. N. Felder, L. Kofman and J. P. Uzan, Phys. Rev. D **76** (2007) 123517; J. F. Dufaux, G. N. Felder, L. Kofman and O. Navros, JCAP **0903** (2009) 001;  
[7] S. Mollerach, D. Harari and S. Matarrese, Phys. Rev. **D 69** (2004) 063002; K. N. Ananda, C. Clarkson and D. Wands, Phys. Rev. D **75**, 123518 (2007); B. Osano et al., JCAP **04** (2007) 003; D. Baumann, P. J. Steinhardt, K. Takahashi and K. Ichiki, Phys. Rev. D **76**, 084019 (2007).  
[8] M. Bastero-Gil, M. Tristram, J. F. Macias-Perez and D. Santos, Phys. Rev. D **77**, 023520 (2008).  
[9] M. Shibata and T. Nakamura, Phys. Rev. **D 52** (1995) 5428; T. W. Baumgarte and S. L. Shapiro, Phys. Rev. **D 59** (1999) 024007.  
[10] J. García-Bellido, M. García-Pérez and A. González-Arroyo, Phys. Rev. **D 67** (2003) 103501.  
[11] J. W. York, Phys. Rev. Lett. **26** (1971) 1656; P. Laguna, H. Kurki-Suonio and R. A. Matzner, Phys. Rev. **D 44** (1991) 3077.  
[12] G. Yoneda and H. Shinkai, Phys. Rev. **D 66** (2002) 124003.  
[13] M. Bastero-Gil, S. F. King and J. Sanderson, Phys. Rev. **D 60** (1999) 103517; G. N. Felder et al., Phys. Rev. Lett. **87** (2001) 011601; G. N. Felder, L. Kofman and A. D. Linde, Phys. Rev. **D 64** (2001) 123517.  
[14] LIGO: <http://www.ligo.caltech.edu>; BBO: <http://universe.nasa.gov/new/program.bbo.html>.

[15] S. Tsujikawa and B. A. Bassett, Phys. Lett. B **536** (2002) 9.

[16] IDRIS: <http://www.idris.fr>; UGRGRID:

<http://ugrgrid.ugr.es>.  
[17] <http://www.llnl.gov/CASC/sundials>.